Modeling and control of a variable-speed wind turbine equipped with permanent magnet synchronous generator

Conference Paper · August 2000

CITATIONS
58

READS
983

4 authors:

Dionysios C Aliprantis
Purdue University
73 PUBLICATIONS **1,932** CITATIONS
SEE PROFILE

Stavros Papathanassiou
National Technical University of Athens
186 PUBLICATIONS **5,997** CITATIONS
SEE PROFILE

Marios Papadopoulos
St George's, University of London
261 PUBLICATIONS **12,620** CITATIONS
SEE PROFILE

A. Kladas
National Technical University of Athens
272 PUBLICATIONS **3,206** CITATIONS
SEE PROFILE

Modeling and control of a variable-speed wind turbine equipped with permanent magnet synchronous generator

D.C. Aliprantis S.A. Papathanassiou M.P. Papadopoulos A.G. Kladas

Purdue University
Electrical and Computer Engineering
Box 130, 1285 Elec. Eng. Building
West Lafayette, IN, 47907-1285, USA
Tel. +1 765 4943396
Email: aliprand@ecn.purdue.edu

National Technical University
Electric Power Division
9, Iroon Polytechniou St.
15780, Zografou – Athens, GREECE
Tel. +301 772 3967
Email: st@power.ece.ntua.gr

ABSTRACT

In this paper the operation of a variable-speed, stall regulated wind turbine equipped with a permanent magnet synchronous generator (PMSG) is examined. The emphasis is placed on the analysis of the electric part of the system, i.e. the electrical generator, the power electronics converters and the control. The operational characteristics of the machine are investigated through a series of computer simulations and the speed control system is designed to maximize the power output and achieve a smooth torque and power profile.

Keywords: wind turbine, variable speed, stall regulated, permanent magnet synchronous generator, control system, simulation.

1 INTRODUCTION

The design of a wind turbine system is a complicated task due to the plethora of parameters involved and the often conflicting requirements, such as the low cost and ruggedness on the one hand, and the good output power quality and dynamic characteristics on the other. In this paper a 25 kW stall regulated, variable speed wind turbine is considered, equipped with a PMSG. The examined WT is currently in the design stage, with the blades and the PMSG already optimized.

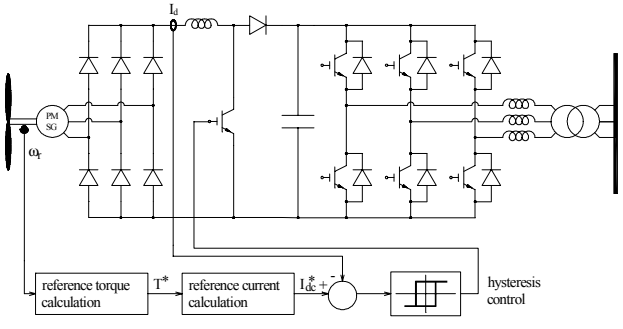

Fig. 1. Configuration of the electrical part.

In order to achieve variable speed operation, a power electronics converter interface is used to connect the generator to the grid, which is illustrated in Fig. 1. The converter consists of an uncontrolled 3-phase diode rectifier, a DC/DC boost converter, a 3-phase PWM voltage source inverter and possibly a step-up transformer. In Fig. 1 the structure of the speed/torque control system is also shown. The measured rotor speed determines the torque reference, which subsequently is used to calculate the DC current reference value. Tracking of this value is performed via the hysteresis control loop of the DC/DC converter. The output PWM inverter regulates the DC voltage at its rated value, as well as the output power factor.

In this paper, the modeling of the generator and power electronics interface is presented, both in the steady state and in dynamic conditions. Average value and detailed switching models are then used to select the parameter values and illustrate the effectiveness of the proposed control system.

2 MODELING OF THE SYSTEM

2.1 Aerodynamic part

The time-average mechanical input power P_m at the shaft of the generator can be calculated from

$$P_m = \frac{1}{2}\rho A V_w^3 C_p(\lambda) \tag{1}$$

where $\rho = 1.25\ kg/m^3$ denotes air density, $A = \pi R^2$ is the area of the rotor, V_w is the wind velocity and $C_p(\lambda)$ is the aerodynamic power coefficient as a function of the tip speed ratio $\lambda = R\omega_m / V_w$. For a given $C_p(\lambda)$, i.e. for the specified blade design, the mechanical power can be plotted as a function of the rotor speed for different values of the wind speed, as shown in Fig. 2. The dashed line represents the conditions for maximum power generation.

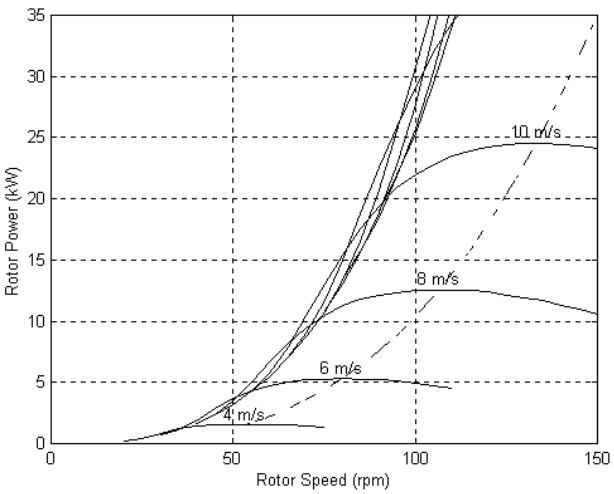

Fig. 2. Mechanical power vs. rotor angular velocity with the wind speed as a parameter.

The rotor aerodynamic torque harmonics due to the tower shadow and wind shear effects must be taken into account in the simulation, since they affect the output power quality. These are modeled as variations of the wind speed acting at the aerodynamic center of each blade. For a 3-blade wind turbine, the distance of each blade from the ground, as a function of its angular position θ_i, is

$$h_i = H_{hub} + cR\sin\theta_i, \quad i = 1\ldots 3 \tag{2}$$

where H_{hub} is the hub height and $c < 1$ defines the distance of the aerodynamic center of the blade from its root. The wind shear, i.e. the variation of wind speed with height, is then given by the following equation for each blade

$$\frac{V_{w,i}(h_i)}{V_w(H_{hub})} = \left(\frac{h_i}{H_{hub}}\right)^a \tag{3}$$

where $a = 0.17$. The tower shadow can be practically described as a sinusoidal reduction of wind speed, as the blades pass in front of the tower, caused by the obstruction of the air flow. Both effects are incorporated in the expression for wind speed at each blade:

$$V_w^{sh}(\theta,t) = V_w(t)\left(\frac{H_{hub} + cR\sin\theta}{H_{hub}}\right)^{0.17} f(\theta) \tag{4}$$

where $f(\theta) = 1 - \Delta V_w \sin\left[\frac{\pi}{2\theta_{sh}}\left(\theta - \left(\frac{3\pi}{2} - \theta_{sh}\right)\right)\right]$

when $\frac{3\pi}{2} - \theta_{sh} + 2k\pi \le \theta \le \frac{3\pi}{2} + \theta_{sh} + 2k\pi, \quad k \in \mathrm{Z}$ and $f(\theta) = 1$, elsewhere. In the above expressions, ΔV_w is the maximum wind speed drop, and θ_{sh} is the effective tower shadow angle. Accordingly, the total input mechanical power on the shaft is equal to

$$P_m = \frac{1}{2}\rho A\sum_{i=1}^{3}\left[V_w^{sh}(\theta_i,t)\right]^3\left[\frac{1}{3}C_p(\lambda_i)\right], \quad i = 1\ldots 3. \tag{5}$$

2.2 Permanent magnet synchronous generator

The generator rotor is equipped with surface mounted permanent magnets and no damping windings. Thus, it is modeled by the following voltage equations in the rotor reference frame (Park's transformation in qd axes) [1], [2]:

$$v_{qs} = -r_s i_{qs} + \frac{d\lambda_{qs}}{dt} + \omega_r\lambda_{ds} \tag{6}$$

$$v_{ds} = -r_s i_{ds} + \frac{d\lambda_{ds}}{dt} - \omega_r\lambda_{qs} \tag{7}$$

$$v_{0s} = -r_s i_{0s} + \frac{d\lambda_{0s}}{dt} \tag{8}$$

$$\lambda_{qs} = -L_{ls} i_{qs} - L_{mq} i_{qs} \tag{9}$$

$$\lambda_{ds} = -L_{ls} i_{ds} + L_{md}\left(-i_{ds} + i'_m\right) \tag{10}$$

$$\lambda_{0s} = -L_{ls} i_{0s} \tag{11}$$

where $v_{qd0s}, i_{qd0s}, \lambda_{qd0s}$ are q, d and 0 axis voltages, currents and flux linkages respectively, i'_m is the equivalent magnetizing current of the permanent magnets, r_s is the stator winding resistance, L_{ls} is the stator leakage inductance, and L_{mq}, L_{md} are the q and d axis magnetizing inductances. The electrical angular velocity ω_r is calculated by

$$T_m - T_e = J\left(\frac{2}{P}\right)\frac{d\omega_r}{dt} \tag{12}$$

where J is the moment of inertia, P is the number of poles, T_m is the mechanical torque on the shaft and T_e the electromagnetic torque, given by

$$T_e = \left(\frac{3}{2}\right)\left(\frac{P}{2}\right)\left(\lambda_{ds} i_{qs} - \lambda_{qs} i_{ds}\right) \tag{13}$$

2.3 Power converters

Detailed models of the three-phase diode rectifier and the boost converter have been developed and used in the simulations, taking into account their switching operation. On the other hand, the switching operation of the output PWM inverter is not represented in detail, assuming that its control is fast enough to maintain the DC link voltage at its reference value. Hence, its operation does not affect the WT dynamics.

3 STEADY STATE OF OPERATION

The steady state operation of the generator can be theoretically predicted by taking into account only the fundamental component of voltages and currents; the low frequency harmonics of the rectifier and the high frequency harmonics of the DC/DC converter are neglected. In the equations that follow, capital letters are used to denote steady state rms values.

Neglecting the commutation phenomena of the diode rectifier, the generator output power factor is constantly equal to unity. Hence, the reactive power is equal to zero, $Q = 0 \Rightarrow V_{ds} I_{qs} = V_{qs} I_{ds}$, and by using the steady state voltage Eqs. (6)-(11), the following relation holds for the *q* and *d* axis currents:

$$L_q I_{qs}^2 + L_d I_{ds}^2 - L_{md} I'_m I_{ds} = 0 \tag{14}$$

Therefore, the *d* and *q* components of the current are constrained by the locus of the ellipse described by Eq. (14), which is independent of the rotor speed. In addition, it introduces an upper limit to the electromagnetic torque that can be developed by the generator. For a non-salient-pole machine, where $L_{mq} = L_{md}$, $L_d = L_{md} + L_{ls}$, this maximum torque can be calculated as

$$T_{e,\max} = \frac{1}{2}\frac{3}{2}\frac{P}{2}\frac{L_{md}^2}{L_d} I'^2_m \tag{15}$$

It is observed that the leakage inductance tends to decrease the maximum torque. This is more obvious in terms of nominal quantities; if the base torque is defined as

$$T_b = S_b \big/ \omega_{mb} \tag{16}$$

where S_b is the base power and ω_{mb} is the nominal angular velocity, it can be proven ([7]) that

$$T_{e,\max} = \frac{1}{2}\frac{1}{X_{d,pu}} T_b \tag{17}$$

The value of the per-unit reactance $X_{d,pu}$ is crucial for the steady state performance of the generator and must be reliably predicted by design calculations. In the case of surface-mounted magnets the leakage inductance can be considerably large.

4 DETAILED SIMULATION RESULTS

The detailed modeling of the generator, the rectifier and the DC/DC converter is very important for obtaining the accurate picture of all the system waveforms (voltages, currents, torque, power, speed). This is required for selecting the ratings of the semiconducting components, as well as for validating the average value models used in the design of the control system and in longer time horizon simulations. In addition, the generator current harmonics give rise to electromagnetic torque oscillations, which may contribute to the fatigue of the mechanical components. Typical simulation results for steady state operating conditions are shown in Fig.3, which includes the generator electromagnetic torque, the stator currents and the rectifier DC current.

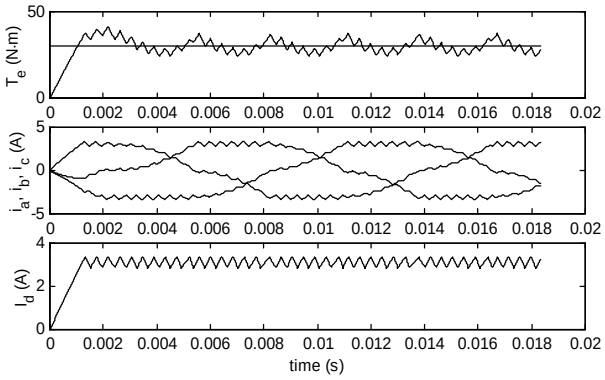

Fig. 3. Simulation results using the detailed switching model.

Using the switching model of the device, the relation between the DC current at the output of the diode bridge and the generator electromagnetic torque was established. This relation, which cannot be computed analytically, is calculated in the form of a look-up table, after a series of simulations, relating torque with current and rotor speed and is directly programmed in the 'reference current calculation' block of Fig. 1.

Subsequently, the possibility of using the rectifier DC inductance for optimizing the chopper switching frequency was investigated. In the short time intervals associated with the chopper operation, the conduction state of the rectifier diodes is fixed and hence the DC choke is series connected to the stator winding of the generator. Due to the high leakage inductance of the winding, it was found that no additional DC choke is required to limit the chopper switching frequency, thus reducing the cost and the weight of the system.

The effect of the hysteresis controller bandwidth, ΔI_{dc}, on the performance of the generator was also investigated. Its amplitude determines the DC current ripple and therefore the amplitude of the high frequency oscillations of the generator electromagnetic torque, but not its mean value. ΔI_{dc} is also inversely proportional to the switching frequency f_s. In [7] it is shown that the following equation holds:

$$f_s = \frac{1}{(2\Delta I_{dc})}\frac{1}{L_d}\frac{\omega_e}{\omega_b}\left(\sqrt{2}V_b\right)\cdot \left(1-\frac{3\sqrt{3}}{\pi}\frac{\omega_e}{\omega_b}\frac{V_b}{V_C}\sqrt{1+\sqrt{1-\frac{T_e}{T_{\max}}}}\right) \quad (18)$$

where ω_e, ω_b are electric and base frequencies, V_b is the generator base voltage, V_C is the DC link capacitor voltage, T_e is the electromagnetic torque and $T_{\max}$ is given by Eq. (17). The above equation correlates excellently with the simulation results and essentially validates the steady state analysis.

5 DESIGN OF THE CONTROL SYSTEM

5.1 Control Strategy

From the power curves shown in Fig. 2, the rotor aerodynamic torque characteristics of Fig. 4 are calculated. The dashed line represents the conditions for maximum wind energy extraction. In the low wind region, the control system is designed so that the turbine operates on this curve. At higher winds, however, the turbine must be protected from over-power and over-torque conditions due to sudden wind gusts. For this purpose, the maximum power curve is followed up to 75 rpm, from which point a parabolic curve leads to the maximum torque $T_{\max}$ = 3.6 kNm at 96 rpm. Following this characteristic, the control takes advantage of the blade stall effect, which effectively reduces the torque and power overshoots. The energy loss due to the early deviation from the optimal power curve is insignificant, since in practice the turbine never operates on the static power curves.

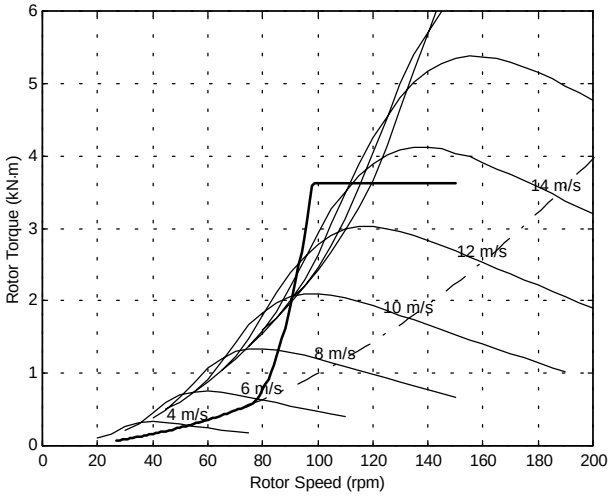

Fig. 4. Torque vs. rotor angular velocity characteristics.

The torque-speed characteristic of Fig. 4 is implemented in the 'reference torque calculation' block of Fig. 1. Hence, the measured rotor speed provides the torque set-point for the generator, whose torque is then regulated by the dc current hysteresis controller.

Besides maximizing the energy output, the control system structure and tuning should enhance the filtering capability of the system, so that the fast variations of the input power, due to

wind fluctuations and aerodynamic torque harmonics, are not transmitted to the output of the WT, [8].

5.2 Average value model

For the evaluation of the control system performance under realistic wind conditions, simulation times of several minutes are often required. The detailed switching model is not suitable for such simulations, nor does it provide any useful information, since the WT dynamic response is determined by the fundamental frequency component of the electric variables. For this purpose, a mean value model is developed, wherein all harmonics are neglected. In addition, the generator torque is considered to be instantaneously controlled, due to the high bandwidth of the hysteresis current controller. This is confirmed in Fig. 5, where the response of the torque to a step change of its reference value is illustrated.

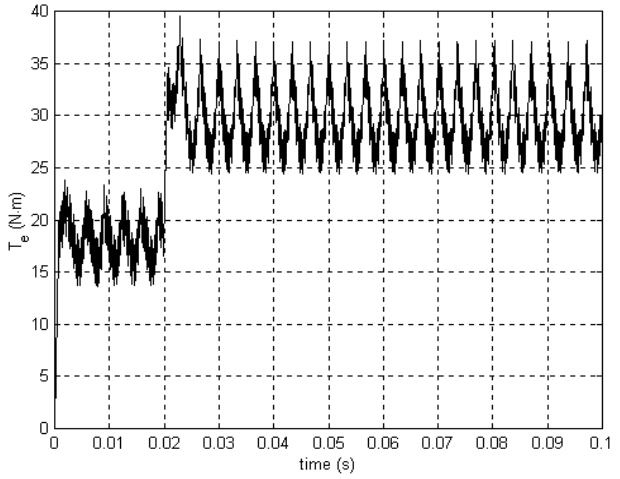

Fig. 5. Electromagnetic torque response to a step change of its reference value.

5.3 Linearized system equations

After determining the speed-torque and torque-DC current characteristics, the control system of Fig. 1 comprises no other controller to be tuned. However, an additional low-pass filter has been included in the rotor speed feedback path, as shown in Fig. 6. Its purpose is to attenuate speed oscillations, which otherwise would be reflected on the generator torque, degrading the output power quality and contributing to the variability of the mechanical torques. The objective of the following analysis is the determination of the time constant T_f of the 1st order low-pass speed filter.

The nonlinear torque-speed characteristic is linearized about an initial operating point ω_0:

$$\Delta T_e(s) = \alpha_0 \cdot \Delta\omega(s) \tag{19}$$

If the mechanical torque is considered to be the input, the linearized system equations are written as follows:

$$\Delta T_e(s) = \frac{1}{\frac{JT_f}{a_0}s^2 + \frac{J}{a_0}s + 1}\Delta T_m(s) \tag{20}$$

$$\Delta\omega(s) = \frac{1}{a_0}\cdot\frac{T_f s + 1}{\frac{JT_f}{a_0}s^2 + \frac{J}{a_0}s + 1}\Delta T_m(s) \tag{21}$$

$$\Delta P_{out}(s) = \frac{\omega_0 a_0 + T_{e0}}{a_0}\cdot\frac{\frac{T_f T_{e0}}{\omega_0 a_0 + T_{e0}}s + 1}{\frac{JT_f}{a_0}s^2 + \frac{J}{a_0}s + 1}\Delta T_m(s) \tag{22}$$

where J is the total inertia of the turbine. In the derivation of the above relations, the PMSG losses are ignored, so that the output power is given by $P_{out} = T_e \cdot \omega$.

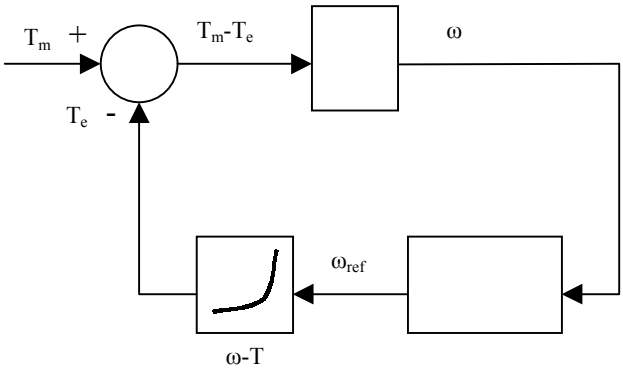

Fig. 6. Control system block diagram.

The low pass filter essentially transforms the system into a second order one. The three transfer functions have the same poles, so they are characterized by the corner frequency

$$\omega_n = \sqrt{\frac{a_0}{JT_f}} \tag{23}$$

and the damping ratio

$$\zeta = \frac{1}{2}\sqrt{\frac{J}{a_0 T_f}} \tag{24}$$

By appropriate selection of the time constant, it is possible to set the poles so that the attenuation is maximized in the cut-off frequency range. The initial operating point is chosen at a high speed, where the system is less damped, and the mechanical stresses, as well as the variation of the output power, are more intense.

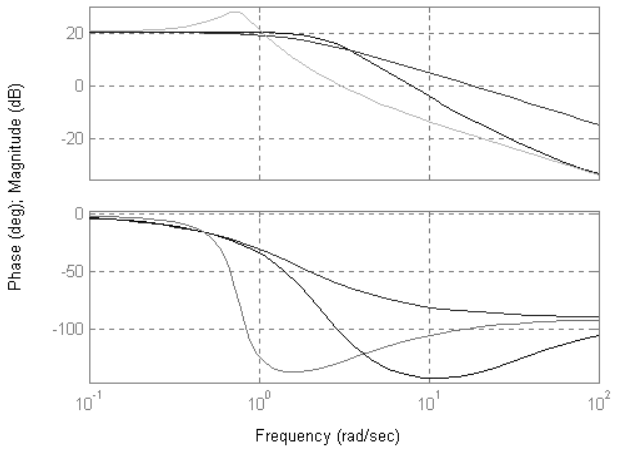

Fig. 7. Bode plot of the output power transfer function, Eq. (22).

An example of the output power transfer function Bode diagram is shown in Fig. 7, where three curves are depicted, for $T_f = 0\,s$, $T_f = 0.3\,s$ and $T_f = 5\,s$. Without the presence of the filter, the attenuation is -20 dB/dec. The introduction of the filter in the feedback path provides additional damping to the undesirable low frequency components, at a rate of -40 dB/dec. Increasing, however, the filter time constant beyond a certain value creates a low frequency resonant peak. A selection of $T_f = 0.2\,s$ is deemed most appropriate.

5.4 Time domain simulations

Using the average value model, a series of simulations in the time domain are performed, to verify the theoretical analysis of the previous section and to fine-tune the filter time constant. In Fig. 8 a step change in the wind speed is simulated. The response of the system exhibits very good damping and the rotor speed reaches its new reference value in less than 2 sec. The ripple observed in the mechanical torque, mainly due to the tower shadow effect, is completely filtered out and does not appear in the electromagnetic torque and output power of the system.

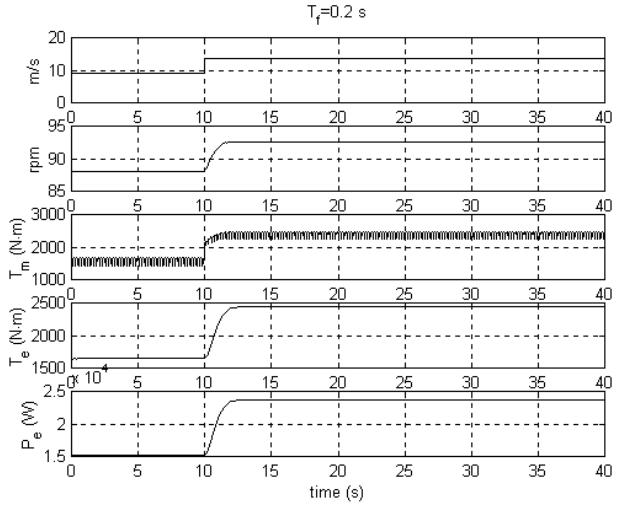

Fig. 8. Step change of wind speed from 9 m/s to 13.5 m/s.

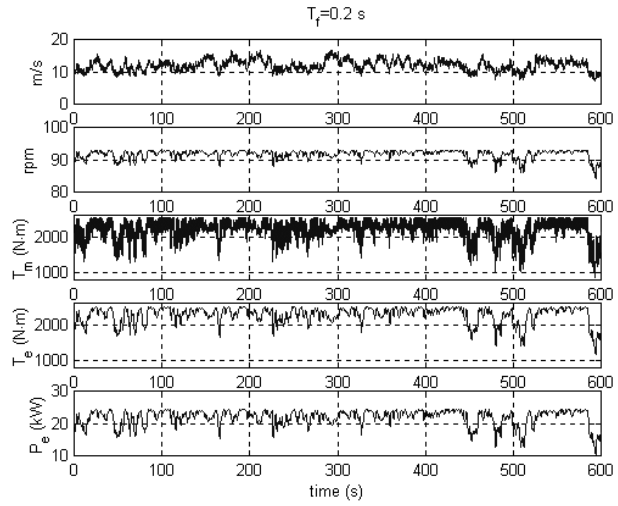

Fig. 9. Stochastic wind simulation (12 m/s average wind speed).

Using the Fourier synthesis method of [6] and a Von Karman spectrum, wind speed time series have been generated in order to simulate the WT response under stochastic wind conditions. In Fig. 9 simulation results are shown using a 10-min, 12 m/s mean speed wind time series. The WT presents good dynamic characteristics, with increased stability margin and filtering capabilities of the fast aerodynamic torque fluctuations.

6 CONCLUSIONS

In this paper steady state and dynamic models were presented and used in the investigation of the performance of a variable speed wind turbine equipped with a PMSG. The computer simulations proved to be a valuable tool in predicting the system behavior, selecting certain of its components and optimizing the speed control system of the WT.

Currently, a scaled-down (2 kW) experimental prototype has been made available and will be used for validating the models developed and testing control strategies, at the Electric Machines Laboratory of NTUA. The outcome of the simulation and experimental work will be utilized in the development of the final 25 kW wind turbine.

7 ACKNOWLEDGEMENT

The authors express their gratitude to the General Secretariat of Research and Technology of Greece for funding the work presented in this paper.

8 REFERENCES

[1] P. C. KRAUSE, O. WASYNCZUK, S. D. SUDHOFF, *Analysis of Electric Machinery*, IEEE Press, 1995.

[2] CHEE-MUN ONG, *Dynamic Simulation of Electric Machinery Using Matlab/Simulink*, Prentice Hall, 1998.

[3] N. MOHAN, T. M. UNDELAND, W. P. ROBBINS, *Power Electronics-Converters, Applications and Design*, 2nd edition, Wiley, 1995.

[4] B. C. KUO, *Automatic Control Systems*, 7th Edition, Prentice Hall International Editions.

[5] S. HEIER, *Grid Integration of Wind Energy Conversion Systems*, Wiley, 1998.

[6] M. SHINOZUKA, C. M. JAN, "Digital Simulation of Random Processes and Its Applications", *Journal of Sound and Vibration*, Vol. 25, Nov. 1972, pp. 111-128.

[7] D. C. ALIPRANTIS, *Modeling and control of a variable speed wind turbine with a permanent magnet synchronous generator*, Diploma Thesis, NTUA, 1999.

[8] S.A. PAPATHANASSIOU, M.P. PAPADOPOULOS, "Dynamic Behavior of Variable Speed Wind Turbines under Stochastic Wind". *IEEE Trans. on Energy Conversion*, Vol. 14, No. 4, Dec. 1999.